Journal Pre-proof

Surface heterostructure induced by TiO_2 modification in Li-rich cathode materials for enhanced electrochemical performances

Xinxin Ran, Jianming Tao, Ziyan Chen, Zerui Yan, Yanmin Yang, Jiaxin Li, Yingbin Lin, Zhigao Huang

PII:	S0013-4686(20)30351-0
DOI:	https://doi.org/10.1016/j.electacta.2020.135959
Reference:	EA 135959
To appear in:	*Electrochimica Acta*
Received Date:	24 December 2019
Accepted Date:	24 February 2020

Please cite this article as: Xinxin Ran, Jianming Tao, Ziyan Chen, Zerui Yan, Yanmin Yang, Jiaxin Li, Yingbin Lin, Zhigao Huang, Surface heterostructure induced by TiO_2 modification in Li-rich cathode materials for enhanced electrochemical performances, *Electrochimica Acta* (2020), https://doi.org/10.1016/j.electacta.2020.135959

GRAPHICAL ABSTRACT

Surface heterostructure induced by TiO_2 modification in Li-rich cathode materials for enhanced electrochemical performances

Xinxin Ran[1,2†], Jianming Tao[1†], Ziyan Chen[1], Zerui Yan[1], Yanmin Yang[1], Jiaxin Li[1], Yingbin Lin*[1,2] and Zhigao Huang[1,2]

1. College of Physics and Energy, Fujian Normal University, Fujian Provincial Engineering Technology Research Center of Solar Energy Conversion and Energy Storage, Fuzhou，350117, China.
2. Fujian Provincial Collaborative Innovation Center for Advanced High-Field Superconducting Materials and Engineering, Fuzhou, 350117, China.

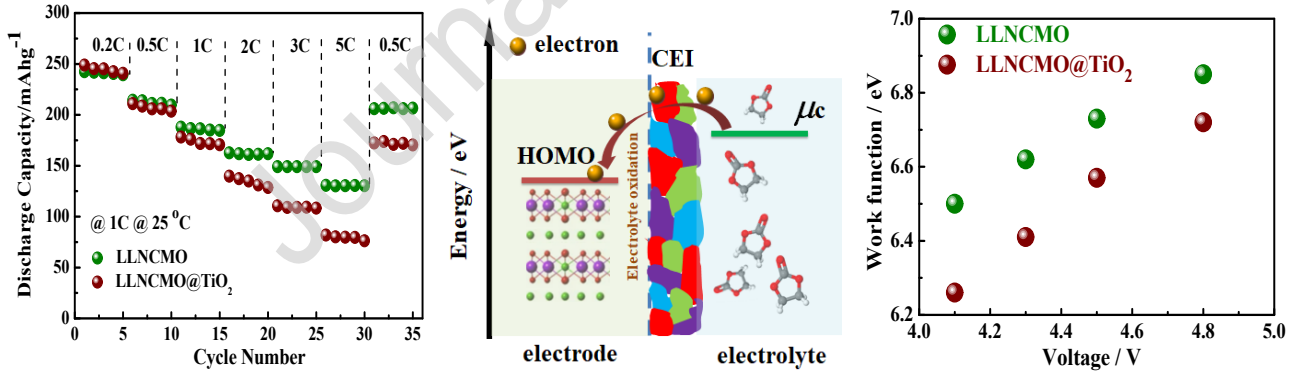

Surface heterostructure induced by TiO_2 modification in Li-rich cathode materials for enhanced electrochemical performances

Xinxin Ran[1,2†], Jianming Tao[1†], Ziyan Chen[1], Zerui Yan[1], Yanmin Yang[1], Jiaxin Li[1], Yingbin Lin*[1,2] and Zhigao Huang[1,2]

1. College of Physics and Energy, Fujian Normal University, Fujian Provincial Engineering Technology Research Center of Solar Energy Conversion and Energy Storage, Fuzhou，350117, China.
2. Fujian Provincial Collaborative Innovation Center for Advanced High-Field Superconducting Materials and Engineering, Fuzhou, 350117, China.

*Corresponding author: Yingbin Lin

Tel: +86-591-2286-8132

Fax: +86-591-2286-8132

E-mail: yblin@fjnu.edu.cn

Abstract

Building stable interfacial structure is highly desirable for high-voltage lithium rich cathode materials for lithium ion batteries. Heterostructure interface should play a crucial role in controlling electrochemical performances of Li-rich oxides. Herein, $Li_{1.2}Ni_{0.13}Co_{0.13}Mn_{0.54}O_2$ nanoparticles are massively prepared via a facile ultrasonic spraying method, followed by surface-modification with TiO_2 ultrathin layer using low-temperature hydrolysis technique. Comparing to pristine $Li_{1.2}Ni_{0.13}Co_{0.13}Mn_{0.54}O_2$, TiO_2-coated composites exhibit better electrochemical performances in terms of rate capability, cycling stability and thermal stability. $Li_{1.2}Ni_{0.13}Co_{0.13}Mn_{0.54}O_2$@$TiO_2$ composites deliver a reversible discharge capacity of 194.9 mAh▪g^{-1} at 25^{o}C and 257.8 mAh▪g^{-1} at 55^{o}C after 100 cycles, while the pristine $Li_{1.2}Mn_{0.52}Ni_{0.13}Co_{0.13}O_2$ only has a discharge capacity of 208.4mAhg^{-1} and 253.9mAhg^{-1} respectively. The TiO_2-coating could reduce the work function of the hybrid composites and efficiently suppress the evolution of a solid electrolyte interface film at the electrode/electrolyte as well as improve thermal stability. Moreover, the built-in electric field originating from the difference in work function at the hetero-junction interface, would also facilitate electron-transfer and Li-ion migration across the hetero-junction interface and consequently robust electrochemical performances.

Keywords**:** lithium-ion batteries; lithium-rich cathode; work function; thermal stability; built-in electric field.

1. Introduction

Rechargeable lithium-ion batteries (LIBs) have attracted increasing attention as the most promising predominant energy-storage technology for portable electronics, electrical vehicles and stationary energy storage owing to their high-energy density, reasonably long-cycle life and environmentally benign [1-3]. The increasing demand for high-energy density LIBs has made the cathode material with high specific capacities to be the primary determinant of the breakthrough for high energy delivery [4,5]. As far, numerous advanced materials are mushrooming and lithium-rich manganese oxides are considered as promising candidates owing to their superior specific capacity (>250 $mAhg^{-1}$), high operation voltage and environmental benignity [6,7]. However, several critical issues including the low initial coulombic efficiency (ICE), severe voltage decay and dissatisfied cyclic stability, should be solved before the commercial application of lithium-rich layered oxides [8, 9]. Up to now, tremendous efforts have been made to relieve these problems including designing hierarchically structure [10,11], doping with isovalent ions [12,13], surface modification [14,15] and so on. Among the available strategies, surface modification is proved to be effective strategy to enhance the electrochemical performances [16-21]. For instance, Liu *et al.* [16] reported Li-rich LNCM@$Ce_{0.8}Sn_{0.2}O_{2-\sigma}$ exhibited an enhanced initial discharge capacity of 315.1 mA h g^{-1} (0.05C) with an excellent initial coulombic efficiency of 92.77% comparing to 79.71% for the pristine one. Hu *et al.* [17] found that $Li_{1.2}Ni_{0.2}Mn_{0.6}O_2$@$LiAlF_4$ delivered a high reversible capacity of 246$mAhg^{-1}$ at 0.1C and excellent rate capability of 133$mAhg^{-1}$ at 5C. It is well established that the improved performances should result from the suppression of side reactions occurring at the interphase between electrodes and electrolyte. The side reactions are strongly dependent on the interfacial properties, which is worth

investigating in terms of enhanced performances. On the other hand, nanosized active materials active materials and uniform-coating of thin layer are highly desirable for surface-modified cathode materials for Li-ion batteries, which could shorten Li-ion diffusion pathway, suppress the side reactions at the electrode/electrolyte interface and facilitate charge migration across electrode/coating-layer interface.

In this work, $Li_{1.2}Ni_{0.13}Co_{0.13}Mn_{0.54}O_2$ (LLNCMO) nanoparticles have been successfully prepared by low-cost ultrasonic spraying under the help of vacuum pump, followed by surface modification with TiO_2 using low-temperature hydrolysis. Vacuum-assisted ultrasonic spraying massively produces well-dispersed hollow spherical precursors and is good for fabricating nanosized materials dependent of sphere wall thickness. Low-temperature hydrolysis is a promising coating technique, which could achieve a well controllable thickness of coating-layer and the uniformity of the coating layer. Titanium butoxide(TBT) is used as Ti precursor for hydrolysis and slow hydrolysis proceeds in alcoholic solution at low ambient temperature, which is beneficial for uniform coating of thin TiO_2-layer on LLNCMO surface. It is found that the TiO_2-coated cathode material exhibits improved electrochemical performances and thermal stability. The potential mechanism behind the improve performances are systematically investigated by electrochemical measurements, work function and well explained based on phenomenological energy-band model.

2. Experimental

2.1 Synthesis of $Li_{1.2}Ni_{0.13}Co_{0.13}Mn_{0.54}O_2$ nanoparticles.

$Li_{1.2}Ni_{0.13}Co_{0.13}Mn_{0.54}O_2$ powders are prepared by a facile ultrasonic spraying followed by high-temperature calcination. Typically, 25.2 mmol $LiCH_3COO{\bullet}2H_2O$ (5% Li excess), 2.6 mmol $Ni(CH_3COO)_2{\bullet}4H_2O$, 2.6 mmol $Co(CH_3COO)_2{\bullet}4H_2O$ and 10.8 mmol $Mn(CH_3COO)_2{\bullet}4H_2O$ are thoroughly dissolved in 100 mL deionized

water. After continuous stirring for 12 h, the resulted solution is ultrasonically atomized and the droplets go through a reactor of 600 ℃ under the help of vacuum pump. Hollow Li-Ni-Co-Mn-O precursors readily form in the reactor under vacuum. The Li-Ni-Co-Mn-O precursors are collected and subsequently calcinated at 900°C for 12 h in air to obtain a homogeneous $Li_{1.2}Ni_{0.13}Co_{0.13}Mn_{0.54}O_2$ nanoparticles (denoted as LLNCMO in the text).

2.2 Synthesis of $Li_{1.2}Ni_{0.13}Co_{0.13}Mn_{0.54}O_2$@$TiO_2$ nanoparticles.

$Li_{1.2}Ni_{0.13}Co_{0.13}Mn_{0.54}O_2$@$TiO_2$ (LLNCMO@TiO_2) nanoparticles are synthesized by a hydrolysis process at low temperature using tetrabutyl titanate (TBT) as Ti sources. In detail, 0.2g as-prepared LLNCMO nanoparticles are dispersed in the mixing solution (40 ml of absolute ethanol and 1 ml of deionized water) at 4 ℃ under vigorous stirring. Afterwards, 0.04 mL TBT solution is added dropwise into above solution. After continuous stirring for 24 h, the obtained precipitates are collected by centrifugation, dried at 80℃ for 6 h and subsequently sintered at 500 ℃ for 3 h to obtain finally product. The synthesis processes of LLNCMO and LLNCMO@TiO_2 nanoparticles are schematically illustrated in Figure1.

2.3. Materials characterization

The crystal structure of the as-prepared composites is studied by powder X-ray diffraction (XRD) using a Rigaku MinFlex II diffractometer with Cu-Kα radiation (λ=1.5406Å). The morphologies of LLNCMO and LLNCMO@TiO_2 powders are analyzed using field-emission scanning electron microscopy (FESEM; HITACHI, SU-8010) equipped with X-ray energy dispersive spectroscopy (EDS). The microstructure of the as-prepared materials is characterized using a transmission electron microscope (TEM, FEI Tecnai G2 F20 S-TWIN). The chemical states of the samples are analyzed by X-ray photoelectron spectroscopy (Thermo Scientific

ESCALAB 250Xi). The TiO_2 content in LLNCMO@TiO_2 composite is determined by inductively coupled plasma (ICP, ICAP700). The surface potentials of LLNCMO and LLNCMO@TiO_2 electrodes are measured by Kelvin probe atomic force microscopy (KPAFM) (Bruker dimension ICON, Germany). Thermogravimetric and differential scanning calorimetric analysis of highly-delithiated LLNCMO and LLNCMO@TiO_2 electrodes, are on a TG-DSC simultaneous thermal analyzer (Netzsch STA449F3). Prior to DSC measurements, the cells are charged to 4.8 V at a current of 0.1 C and then disassembled in an argon-filled glove box. The cathode materials including acetylene black and PVDF are scraped from the Al current collector, and subsequently sealed in a stainless-steel pan.

2.4 Cell fabrication and characterization

The electrochemical experiments are performed using CR2025 half-cells which are assembled in an Ar-filled glove box with lithium foil as a counter electrode. The cathode slurry is prepared by mixing 80 wt.% active material (LLNCMO or LLNCMO@TiO_2) with 10 wt.% polyvinylidene fluoride (PVDF) and 10 wt.% super-P in N-methy1-2-pyrrolidone (NMP). The formed homogeneous slurry is then cast onto an aluminum foil and subsequently dried at 120 °C in vacuum for 12 h. The loading density of the active materials is approximately of 2 mg•cm^{-2}. The cathode and anode electrodes are separated by a microporous Celgard 2400 membrane. The electrolyte is 1 M $LiPF_6$ in dimethyl carbonate (DMC)-ethylene carbonate (EC) (1:1 in volume). Galvanostatic charge-discharge measurements are carried out in the voltage range of 2.0 − 4.8 V on a LAND test system (CT2001A, China). Cyclic voltammetry (CV) are recorded with BT2000 Arbin instrument at a scan rate of 0.1 mVs^{-1}. Electrochemical impedance spectra of the cells are recorded in the frequency range of 100 kHz to 10 mHz with AC amplitude of 5 mV on a Zahner Zennium

IM6 electrochemical workstation.

3. Results and discussion

The morphologies of LLNCMO and LLNCMO@TiO_2 particles are characterized by SEM. As shown in Fig 2(a,b), both the pristine and TiO_2-coated composites are consisted with well-crystallized nanoparticles with an average diameter of ~200 nm. However, the crystal faces and boundaries of LLNCMO particles become slight blurry due to the deposition of TiO_2 nanoparticles on the cathode material. Figure 2(c) shows XRD patterns of the LLNCMO and LLNCMO@TiO_2 composites. All diffraction peaks are assigned to hexagonal α -$NaFeO_2$ structure with the R-3m space group except for the weak peaks around 20°-23°, which correspond to the $LiMn_6$ superstructures of monoclinic Li_2MnO_3 unit cell with space group C2/m (JCPDS No. 21-1272) [22]. The distinct splitting of the pair reflections (006)/(102) and (108)/(110) suggests the highly ordered hexagonal structure of LLNCMO powder [23]. A weak peak at 2θ≈25.3° LLNCMO@TiO_2 composites is indexed to the (101) crystal plane of anatase TiO_2 [24, 25]. To further confirm the presence of TiO_2 on LLNCMO surface, the high-magnification TEM images of LLNCMO@TiO_2 samples are presented in Fig. 2(d-f). As can be found, a distinguishable coating-layer with a thickness of ~6 nm is deposited on LLNCMO surface. The pristine LLNCMO demonstrates clear lattice fringes (003) with a d-spacing of 0.47 nm [26]. The distance between the lattice fringes is ~0.35 nm, corresponding to the (101) planes of anatase TiO_2 crystallite [27]. The chemical composition of coating-layer is further examined by the EDS elemental mapping. Analysis from the mapping in Fig. 2 (g-l) reveals the uniform distribution of Ti element on the LLNCMO surface. Precise amounts of Ni, Co, Mn and Ti elements are tested by the inductively coupled plasma (ICP) technique and the corresponding TiO_2 content in composite is evaluated as 4.6%, which reveals

a good consistency between the reality and calculation of Ti element.

The initial charge/discharge curves of LLNCMO and LLNCMO@TiO_2 are plotted in Fig. 3(a) in the voltage range of 2.0-4.8 V at 0.2C (1C=300 $mAhg^{-1}$). As depicted in Fig. 3(a), the initial charge curves of both samples demonstrate an oblique platform of 3.7-4.5V related to the oxidation of Ni^{2+} and Co^{3+}, followed by a typical plateau of 4.5-4.8V due to the simultaneous removal of oxygen from Li_2MnO_3 [28,29]. LLNCMO electrode delivers an initial discharge capacity of 259.4$mAhg^{-1}$ with initial coulombic efficiency (ICE) of 76.1% while LLNCMO@TiO_2 exhibits a discharge capacity of 254.6 $mAhg^{-1}$ with higher ICE of 82.4%. The oxidation of electrolyte at the high cutoff voltage should be responsible for the low initial coulomb efficiency [30]. The TiO_2-coating effectively suppresses such decomposition reaction and promotes Li-ion delivery in lithium-rich oxide materials.

Figure 3 (b) shows the rate capability of the pristine and TiO_2-coated LLNCMO cathode. All the samples are performed an activated procedure at 0.1 C for 2 cycles before the testing. It can be observed that LLNCMO@TiO_2 electrode demonstrates better rate capability especially at high rates. The LLNCMO@TiO_2 delivers a discharge capacity of 130.3$mAhg^{-1}$ while the pristine is only 76.2$mAhg^{-1}$. When the discharge rate is returned from 5 C to 0.5C, LLNCMO@TiO_2 electrodes could also recover to higher capacity. The enhanced rate performance of LLNCMO@TiO_2 is largely attributed to a faster Li-ion diffusion across the interface [31]. Fig. 3 (c,d) shows the discharge curves of the LLNCMO and LLNCMO@TiO_2 electrodes at 0.2, 0.5, 1, 2, 3 and 5C respectively. The discharge capacities of both electrodes decrease with the increasing of the current density, which is mainly attributed to increased polarization and electrode overpotential [32]. In comparison with the pristine electrode, LLNCMO@TiO_2 electrode delivers a slower pace in discharging voltage

plateau because of weaker polarization. The obtained results suggest that the coating strategies would effectively suppress the interfacial reaction between the electrolyte and cathode materials, reducing the interfacial resistance. On the other hand, the improved rate capability of might be beneficial from the enhanced electronic conductivity of composites by introducing defects into TiO_2 semiconductor such as oxygen vacancies during the calcination process.

A comprehensive investigation of the benefits of TiO_2 coating also involved cycling test at 25 ^oC and 55^oC. As can be found in Fig. 4(a), stable capacities of 208.4 and 194.9 $mAhg^{-1}$ with retentions of 62.6% and 79.6% are obtained after 100 cycles at 25^oC at 1C for LLNCMO and LLNCMO@TiO_2 electrodes, respectively. In the case of 55^oC(Fig. 4(b)), LLNCMO electrode dropped dramatically to 253.9 $mAhg^{-1}$ with capacity retention of 53.2% after 100 cycles while LLNCMO@TiO_2 electrode delivers discharge capacity of 265.5 $mAhg^{-1}$ with capacity retention of 72.1 %. The capacity maintenance improvement should benefit from the suppressed side reaction between cathode material and acidic liquid electrolyte at high voltage due to the protective effect of the TiO_2-coating layer [33,34]. Fig. 4(c,d) depicts the cyclic voltammetry (CV) curves of the LLNCMO and LLNCMO@TiO_2 electrodes at a scan rate of 0.1 mV s^{-1}. LLNCMO@TiO_2 electrode has smaller difference (Δ V=0.66V) between the reduction peak and the oxidation peak than that (Δ V=0.70V) of LLNCMO electrode, indicating that TiO_2-coating reduce electrode polarization and enhance reversibility of the Li-ion extraction/insertion process [35,36]. From the second cycle onward, the CV curves overlap of LLNCMO@TiO_2 electrode is better than that of LLNCMO electrode, indicating that the TiO_2-coating is helpful to improve lithiation/delithiation reversibility and cycle stability.

To further investigate the potential mechanism behind the improved performance

of LLNCMO@TiO_2 samples, electrochemical independence spectra (EIS) of LLNCMO and LLNCMO@TiO_2 at full charged state are carried out after 100 cycles. As shown in Fig. 5(a), both EIS curves display a straight line at the low frequency region and a depressed semicircle at the high frequency region, reflecting the charge-transfer process and the Li-ion diffusion in active material, respectively. According to the equivalent circuit presented in the inset, the charge-transfer resistances (R_{ct}) of LLNCMO and LLNCMO@TiO_2 electrodes are calculated to be 121.5 and 33.8 Ω respectively. A higher R_{ct} generally indicates slower kinetics of the faradic reaction [37], suggesting that TiO_2-coating would effectively suppress the side reactions of the cathode material with electrolyte upon cycling. To quantitatively identify the effect of TiO_2-coating on Li-ion kinetic diffusion in cathode material, the Li-ion diffusion coefficient (D_{Li}+) is determined by the galvanostatic intermittent titration technique (GITT). The GITT data is collected with a repeated pulse current of 0.2 C and a long relaxation time interval of 40 min in order to obtain a quasi-steady state. Figure 5(b, c) shows the GITT curve of LLNCMO and LLNCMO@TiO_2 samples in the initial charge process. The Li-ion diffusion coefficient is calculated as follows [38,39]

$$D = \frac{4}{\pi\tau}\left(\frac{m_B V_M}{M_B S}\right)^2\left(\frac{\Delta E_s}{\Delta E_\tau}\right)^2 \quad (1)$$

where τ is the pulse duration, m_B and M_B are the mass and molar weight of active cathode material, respectively, S is the surface area of the electrode, V_M is the electrode molar volume of LLNCMO (cm^3), ΔE_S and ΔE_τ can be read directly from the GITT profiles. As can be seen from the calculated D_{Li}+ shown in Fig. 5(d), LLNCMO@TiO_2 electrode exhibits larger Li-ions diffusion coefficient than that of LLNCMO electrode, further indicating TiO_2-coating indeed facilitate Li-ion diffusion in the composite by enhancing the structure stability of the interface.

To study the potential mechanism of the improved Li-ion diffusion kinetics by TiO_2-coating, EIS measurements of LLNCMO and LLNCMO@TiO_2 electrodes are performed at the full charge state from 0°C to -30°C (Figs. 6(a,b)). The EIS profiles are fitted according to the equivalent circuit shown in Fig.5(a). The fitted results reveal that LLNCMO demonstrates a more pronounced effect on charge-transfer behavior at the electrode-electrolyte interface with the increasing temperature. The activation energy (Δ G) of lithium-ion insertion/extraction in LLNCMO and LLNCMO@TiO_2 is calculated as follows[40]

$$\log R_{ct} = \log A + \frac{\Delta G - R}{2.303RT} \quad (2)$$

where ΔG means the activation energy, R is the gas constant, and A is a temperature-independent constant. Based on the temperature dependence of log Rct from 0°C to -30°C depicted in Fig. 6(c), the activation energy ΔG for LLNCMO and LLNCMO@TiO_2 are evaluated as 32.82 $KJmol^{-1}$ and 19.98 $KJmol^{-1}$, respectively. Lower activation energy reflects faster Li-ion diffusion [40], which is good agreement with the analysis of electrochemical measurements.

To get insight into the potential mechanism behind the improved performances from the viewpoint of the interfacial effect, the physical properties of the composites are investigated using Kelvin probe atomic force microscopy. The working electrodes including LLNCMO and LLNCMO@TiO_2 powders (Fig.7(a)), are galvanostatic charged to 4.1, 4.3, 4.5, 4.8V at 0.1 C and subsequently disassembled in an argon-filled glove box. The surface potentials of LLNCMO and LLNCMO@TiO_2 powders at different charged state are measured and the corresponding work function is calculated (Figs. 7(b,c). Work function defined with respected to the Fermi energy of the electrons, reflects the kinetic energy of the electrons to overcome the barrier and thus escape the composite [41]. As compared in Fig.7(d),

$Li_{1.2-x}Ni_{0.13}Co_{0.13}Mn_{0.54}O_2@TiO_2$ has smaller work function than that of $Li_{1.2-x}Ni_{0.13}Co_{0.13}Mn_{0.54}O_2$ at 4.1, 4.3, 4.5 and 4.8 V respectively during the charging process. Smaller work function indicates high-conductivity of composites, confirming the better rate capability induced by surface-modification with TiO_2.

The reduction of work function for LLNCMO by TiO_2-coating is phenomenologically explained based on energy-band model [42]. As shown in Fig. 8(a), LLNCMO and TiO_2 share a common vacuum level, but their Fermi levels are not aligned due to the different work functions. Once the two composites are brought into electrical contact in Fig.8(b), electrons tend to transfer from TiO_2 with smaller work function to LLNCMO with larger work function until the Fermi levels are aligned [43]. As a result, LLNCMO@TiO_2 has smaller work function than that of the LLNCMO composite. Although Fermi-level of the electrode is not constant because the chemical potential of LLNCMO is changing during the charging process, LLNCMO@TiO_2 exhibits smaller work function than that of LLNCMO on a whole. As Goodenough reported [44], the electrolyte would be oxidized when Fermi level of cathode is below the highest occupied molecular orbital of carbonate electrolyte (5.6 eV). Therefore, the oxidation of the electrolyte could be effectively suppressed by reducing the difference in work function between cathode material and the electrolyte. Deduction from the energy level shown in Fig.8(c) indicates TiO_2-coating could reduce the difference in work function and the cycling capability of LLNCMO@TiO_2 is correspondingly improved. Fig. 8(d) shows DSC profiles of the LLNCMO and LLNCMO@TiO_2 electrodes at the full charged state of 4.8 V without removal of the electrolyte. A distinct exothermic peak around 210℃ is observed, corresponding to the decomposition of electrolyte and electrolyte oxidation caused by oxygen released from Li-excess layered oxides. In comparison, LLNCMO@TiO_2 has

thermal decomposition temperature of ~216.1℃, which is higher than that of bare LLNCMO nanoparticles (~209.9℃). Meanwhile, LLNCMO@TiO_2 electrode has relatively lower heat generation of 1.03mWmg^{-1} comparing to the pristine one. The thermal safety of the full-charged Li-excess layered oxides is strongly related to the side reactions between highly oxidative cathode and electrolyte, resulting in a large amount of thermal and gas release [45]. Therefore, TiO_2-coating layer separates the active material from vigorous side reactions and consequently enhance the structural stability at active material/electrolyte interface. Novelty, a built-in electric field (E) is expected to be set up between positively-charged TiO_2 and negatively-charge LLNCMO because of electron transfer, shown in Fig.8(b). Such built-in electric field could facilitate Li-ion diffusion and electron transfer across the LLNCMO/TiO_2 hetero-junction interface, consequently improving the Li-ion diffusion kinetics and rate capability.

In order to identify the positive effects of TiO_2-coating on the enhanced interfacial stability of the cathode materials, XPS analyses are carried out for the LLNCMO and LLNCMO@TiO_2 electrodes after the 100th cycle. As displayed in Fig. 9 (a, b), the O1s could be fitted with four separate peaks around at 529.7, 531.3, 532 and 529.7 eV, which are assigned to C=O, oxygenated deposited species, Li_2CO_3 and electrolyte oxidation products, respectively [46,47]. As a negative product of side reaction, Li_2CO_3 with poor electronic/ionic conductivity increase the electrode polarization and deteriorate the Li-ion diffusion kinetics [48,49]. Comparing to LLNCMO electrodes, LLNCMO@TiO_2 has relatively lower Li_2CO_3 and higher oxygenated deposited species, indicating that TiO_2-coating could efficiently suppress side reaction between the electrolyte and LLNCMO. The obtained results are consistent with the analysis of the EIS and GITT measurements. The C 1s spectra

(Fig. 9(c, d)) of the samples further certify the reduction of Li_2CO_3 species by TiO_2-coating during the charging/discharging process. On the other hand, the side reaction between the electrolyte and LLNCMO also induces the surface-structure disorder of LLNCMO particles, leading to the change in the valence state of metal ions [50]. The fitting of the Mn2p spectrum is shown in Fig. 7(a, b), and the chemical states of Mn in $Li_{1.2}Ni_{0.13}Co_{0.13}Mn_{0.54}O_2$ and $Li_{1.2}Ni_{0.13}Co_{0.13}Mn_{0.54}O_2$@$TiO_2$ can be assigned to Mn^{2+} (2p3/2 641.1 eV), Mn^{3+} (2p3/2 641.9 eV), Mn^{4+} in $Li_{1.2}Ni_{0.13}Co_{0.13}Mn_{0.54}O_2$ (2p3/2 642.7 eV) and Mn^{4+} in Li_2MnO_3 (2p3/2 643.8 eV) respectively [46, 51-53]. It is found that LLNCMO electrode has relatively higher Mn^{2+} content and lower Mn valence than those in LLNCMO@TiO_2 electrode. The higher Mn^{4+}/Mn^{2+} ratio further confirms that TiO_2-coating could not only alleviate the reduction of Mn valence but also suppress the layered-spinel transition induced by oxygen release during cycling [46, 54, 55].

Fig.10 (a-d) shows F 1s, (c, d) P 2p XPS spectra of LLNCMO and LLNCMO@TiO_2 electrodes after 100 charge/discharge cycles, confirming the existence of LiF, C-F and $Li_xPO_yF_z$ species in CEI film on the electrodes. LiF and $Li_xPO_yF_z$ species could be readily generated by the decomposition of $LiPF_6$ [56, 57]. The relative content of elements in LLNCMO and LLNCMO@TiO_2 electrodes is shown in Fig.10 (e, f), revealing the decreasing contents of C and F associated with CEI layer. The obtained results and the decreasing contents of $Li_xPO_yF_z$ species indicate that TiO_2-coating could effectively suppress the decomposition of $LiPF_6$ upon cycling. On the other hand, some poor-conductivity species including LiF and Li_2CO_3 also result in the inferior electrochemical performances [58, 59]. Thereby, the electrochemical performances are correspondingly enhanced by surface-modification with TiO_2.

4. Conclusions

$Li_{1.2}Mn_{0.54}Ni_{0.13}Co_{0.13}O_2$ nanoparticles have been successfully prepared are prepared by ultrasonic spraying technique under partial vacuum condition, and subsequently surface modification with TiO_2 using low-temperature hydrolysis. Comparing to $Li_{1.2}Mn_{0.54}Ni_{0.13}Co_{0.13}O_2$, $Li_{1.2}Mn_{0.54}Ni_{0.13}Co_{0.13}O_2$@$TiO_2$ exhibits excellent electrochemical performance in terms of rate capability, cycling stability and cycling stability. TiO_2 on the surface of $Li_{1.2}Mn_{0.54}Ni_{0.13}Co_{0.13}O_2$ could segregate the electrolyte and active materials, and also prevent active materials against HF-attacking. Furthermore, the built-in electric field existed in hetero-junction interfaces would be beneficial for facilitate electron-transfer and Li-ion migration, resulting in improved electrochemical performance.

Acknowledgements

X. X. Ran and J. M. Tao contributed equally to this work. This work is supported by a grant from National Natural Science Foundation of China (No. 61804030), Solar Energy Conversion & Energy Storage Engineering Technology Innovation Platform (No. 2018L3006) and Natural Science Foundation of Fujian Province (Grant No. 2017J01035).

References

[1] B. Diouf, R. Pode, Potential of lithium-ion batteries in renewable energy, ***Renewable Energy***, 76 (2015) 375-380.

[2] J. W. Choi, D. Aurbach, Promise and reality of post-lithium-ion batteries with high energy densities, ***Nat. Rev. Mater.***, 1 (2016) 16013-16028.

[3] G. E. Blomgren, The development and future of lithium ion batteries. ***J. Electrochem. Soc.***, 164 (2017) A5019-A5025.

[4] J. L. Shi, D. D. Xiao, M. Y. Ge, X. Q. Yu, Y. Chu, X. J. Huang, X. D. Zhang, Y. X. Yin, X. Q. Yang, Y. G. Guo, L. Gu, L. J. Wan, High-capacity cathode material with high voltage for Li-ion batteries, ***Adv. Mater.***, 30 (2018) 1705575.

[5] U. H. Kim, D. W. Jun, K. J. Park, Q. Zhang, P. Kaghazchi, D. Aurbach, D. T. Major, G. Goobes, M. Dixit, N. Leifer, C. M. Wang, P. Ya, D. Ahn, K. H. Kim. S. Yoon, Y. K. Sun, Pushing the limit of layered transition metal oxide cathodes for high-energy density rechargeable Li ion batteries, ***Energy Environ. Sci.***, 11 (2018) 1271-1279.

[6] J. Hong, H. Gwon, S.-K. Jung, K. Ku, K. Kang, Review−lithium-excess layered cathodes for lithium rechargeable batteries, ***J. Electrochem. Soc.***, 162 (2015) A2447−A2467.

[7] H. G. Pan, S. M. Zhang, J. Chen, M. X. Gao, Y. F. Liu, T. J. Zhu, Y. Z. Jiang, Li- and Mn-rich layered oxide cathode materials for lithium-ion batteries: a review from fundamentals to research progress and applications, ***Mol. Syst. Des. Eng.***, 3 (2018) 748-803.

[8] E. M. Erickson, F. Schipper, T. R. Penki, J. Y. Shin, C. Erk, F. F. Chesneau, B. Markovsky, D. Aurbach, Recent advances and remaining challenges for lithium ion battery cathodes: II. lithium-rich, $xLi_2MnO_3\bullet(1-x)LiNi_aCo_bMn_cO_2$ batteries

and energy storage, ***J. Electrochem. Soc.***, 164 (2017) A6341-A6348.

[9] P. K. Nayak, E. M. Erickson, F. Schipper, T. R. Penki, N. Munichandraiah, P. Adelhelm, H. Sclar, F. Amalraj, B. Markovsky, D. Aurbach, Review on challenges and recent advances in the electrochemical performance of high capacity Li-and Mn-rich cathode materials for Li-ion batteries, ***Adv. Energy Mater.***, 8 (2018) 1702397.

[10] Y. Zhang, W. S. Zhang, S. Y. Shen, X. H. Yan, A.M. Wu, J. W. Yin, J. L. Zhang, Hollow porous bowl-shaped lithium-rich cathode material for lithium-ion batteries with exceptional rate capability and stability, ***J. Power Sources***, 380, (2018) 164-173.

[11] M. Chen, X. J. Jin, Z. Chen, Y. T. Zhong, Y. H. Liao, Y. C. Qiu, G. Z. Cao, W. S. Li, A cross-like hierarchical porous lithium-rich layered oxide with (110)-oriented crystal planes as a high energy density cathode for lithium ion batteries, ***J. Mater. Chem. A***, 7 (2019) 13120-13129.

[12] G. R. Chen, J. An, Y. M. Meng, C. Z. Yuan, B. Matthews, F. Dou, L. Y. Shi, Y. F. Zhou, P. G. Song, G. Wu, D. S. Zhang, Cation and anion Co-doping synergy to improve structural stability of Li- and Mn-rich layered cathode materials for lithium-ion batteries, ***Nano Energy,*** 57 (2019) 157-165.

[13] P. Vanaphuti, J. J. Chen, J. Y. Cao, K. Bigham, B. Chen, L. F. Yang, H L. Chen, Y. Wang. Enhanced electrochemical performance of the lithium-manganese-rich cathode for Li-ion batteries with Na and F codoping, ***ACS Appl. Mater. Interfaces,*** 11 (2019) 37842-37849.

[14] J. C. Zheng, Z. Yang, P. B. Wang, L. B. Tang, C. S. An, Z. J. He, Multiple linkage modification of lithium-rich layered oxide $Li_{1.2}Mn_{0.54}Ni_{0.13}Co_{0.13}O_2$ for lithium ion battery, ***ACS Appl. Mater. Interfaces,*** 10 (2018) 31324-31329.

[15] F. D. Yu, L. F. Que, C. Y. Xu, M. J. Wang, G. Sun, J. G. Duh, Z. B. Wang. Dual conductive surface engineering of Li-Rich oxides cathode for superior high-energy-density Li-ion batteries, ***Nano Energy,*** 59 (2019) 527-536.

[16] Y. Liu, Z. Yang, J. Li, B. Niu, K, Yang, F, Kang, A novel surface-heterosturctured $Li_{1.2}Mn_{0.54}Ni_{0.13}Co_{0.13}O_2@Ce_{0.8}Sn_{0.2}O_{2-\sigma}$ cathode material for Li-ion batteries with improved initial irreversible capacity loss, ***J. Mater. Chem. A***, 6 (2018) 13883-13893.

[17] S. Q. Zhao, B. Sun, K. Yan, J. Q. Zhang, C. Y. Wang, G. X. Wang, Aegis of lithium-rich cathode materials via heterostructured $LiAlF_4$ coating for high-performance lithium-ion batteries, ***ACS Appl. Mater. Interfaces***, 10 (2018) 33260-33268.

[18] X. H. Zhang, X. Xie, R. Z. Yu, J. R. Zhou, Y. Huang, S. Cao, Y. Wang, K. Tang, C. Wu, X. Y. Wang. Improvement of the cycling stability of Li-rich layered Mn-based oxide cathodes modified by nanoscale $LaPO_4$ coating, ***ACS Appl. Energy Mater.***, 2 (2019) 3532-3541.

[19] Y. Gao, R. L. Patel, K. Y. Shen, X. Wang, R. L. Axelbaum, X. Liang, Boosting the electrochemical performance of $Li_{1.2}Mn_{0.54}Ni_{0.13}Co_{0.13}O_2$ by atomic layer-deposited CeO_2 coating, ***ACS Omega***, 3 (2018) 906-916.

[20] C. C. Qin, J. L. Cao, J. Chen, G. L. Dai, T. F. Wu, Y. B. Chen, Y. F. Tang, A. D. Li, Y. F. Chen, Improvement of electrochemical performance of nickel rich $LiNi_{0.6}Co_{0.2}Mn_{0.2}O_2$ cathode active material by ultrathin TiO_2 coating, ***Dalton Trans.***, 45 (2016) 9669-9675

[21] J. Y. Mun,J. H. Park, W. Choi, A. Benayad, J. H. Park, J. M. Lee, S. G. Doo, S. M. Oh, New dry carbon nanotube coating of over-lithiated layered oxide cathode for lithium ion batteries, ***J. Mater. Chem. A***, 2 (2014) 19670-19677.

[22] R. Shunmugasundaram, R.S. Arumugam, J. R. Dahn, High capacity Li-rich positive electrode materials with reduced first-cycle irreversible capacity loss**,** ***Chem. Mater.***, 27 (2015) 757-767.

[23] H.Z. Zhang, Q.Q. Qiao, G.R. Li, S.H. Ye, X.P. Gao, Surface nitridation of Li-rich layered $Li(Li_{0.17}Ni_{0.25}Mn_{0.58})O_2$ oxide as cathode material for lithium-ion battery, ***J. Mater. Chem.***, 22 (2012) 13104-13109.

[24] Y. Liang, N. Li, F. Li, Z. Xu, Y. Hu, M. Jing, K. Teng, X. Yan, J. Shi, Controllable nitrogen doping and specific surface from freestanding TiO_2@carbon nanofibers as anodes for lithium ion battery, ***Electrochim. Acta***, 297 (2019) 1063-1070.

[25] Y. Chen, Y. Zhang, B. Chen, Z. Wang, C. Lu, An approach to application for $LiNi_{0.6}Co_{0.2}Mn_{0.2}O_2$ cathode material at high cutoff voltage by TiO_2 coating, ***J. Power Sources***, 256 (2014) 20-27.

[26] Z. Ma, J. C. Huang, J. B. Quan, L. Mei, J. Guo, D. C. Li, Improved electrochemical performances of layered lithium rich oxide $0.6Li[Li_{1/3}Mn_{2/3}]O_2 \cdot 0.4LiMn_{5/12}Ni_{5/12}Co_{1/6}O_2$ by Zr doping, ***RSC Adv.***, 6 (2016) 20522-20531.

[27] H. Yang, K. Du, G. R. Hu, Z. D. Peng, Y. B. Cao, K. P. Wu, Y. Lu, X. Y. Qi, K. C. Mu, J. L. Wu, Graphene@TiO_2 co-modified $LiNi_{0.6}Co_{0.2}Mn_{0.2}O_2$ cathode materials with enhanced electrochemical performance under harsh conditions, ***Electrochim. Acta***, 289 (2018) 149-157.

[28] J. Zhang, Z. Lei, J. Wang, Y. NuLi, J. Yang, Surface Modification of $Li_{1.2}Ni_{0.13}Co_{0.13}Mn_{0.54}O_2$ by Hydrazine Vapor as Cathode Material for Lithium-Ion Batteries, ***ACS Appl. Mater. Interfaces***, 7 (2015) 15821-15829.

[29] J. Kong, C. Wang, X. Qian, G. Tai, A. Li, D. Wu, H. Li, F. Zhou, C. Yu, Y. Sun,

D. Jia, W. Tang, Enhanced electrochemical performance of $Li_{1.2}Mn_{0.54}Ni_{0.13}Co_{0.13}O_2$ by surface modification with grapheme-like lithium-active MoS_2, ***Electrochim. Acta***, 174 (2015) 542-550.

[30] Y. Wu, A. Vadivel Murugan, A. Manthiram, Surface modification of high capacity layered $Li[Li_{0.2}Mn_{0.54}Ni_{0.13}Co_{0.13}]O_2$ cathodes by $AlPO_4$, ***J. Electrochem. Soc.***, 155 (2008) A635-A641.

[31] X. F. Wen, K. Liang, L. Y. Tian, K. Y. Shi, J. S. Zheng, Al_2O_3 coating on $Li_{1.256}Ni_{0.198}Co_{0.082}Mn_{0.689}O_{2.25}$ with spinel-structure interface layer for superior performance lithium ion batteries, ***Electrochim. Acta***, 260 (2018) 549-556.

[32] F. X. Ding, J. L. Li, F. H. Deng, G. F. Xu, Y. Y. Liu, K. Yang, F. Y. Kang, Surface heterostructure induced by $PrPO_4$-modifying in $Li_{1.2}[Mn_{0.54}Ni_{0.13}Co_{0.13}]O_2$ cathode material for high performance lithium ion batteries with mitigating voltage decay, ***ACS Appl. Mater. Interfaces***, 9 (2017) 27936-27945.

[33] H. Liu, C. Chen, C. Du, X. He, G. Yin, B. Song, P. Zou, X. Cheng, Y. Ma, Y. Gao, Lithium-rich $Li_{1.2}Ni_{0.13}Co_{0.13}Mn_{0.54}O_2$ oxide coated by Li_3PO_4 and carbon nanocomposite layers as high performance cathode materials for lithium ion batteries, ***J. Mater. Chem. A***, 3 (2015) 2634-2641.

[34] S. M. Zhang, H. T. Gu, T. Tang, W. B. Du, M. X. Gao, Y. F. Liu, D. C. Jian and H. G. Pan, In-situ encapsulation of nanoscale Er_2O_3 phase to drastically suppress voltage fading and capacity degradation of Li and Mn-rich layered oxide cathode for lithium-ion batteries, ***ACS Appl. Mater. Interfaces,*** 9 (2017) 33863-33875.

[35] H. Zhou, Z. Yang, D. Xiao, K. Xiao, J. Li, An electrolyte to improve the deep chargedischarge performance of $LiNi_{0.8}Co_{0.15}Al_{0.05}O_2$ cathode, ***J. Mater. Sci.: Mater. Electron.***, 29 (2018) 6648–6659.

[36] C. X. Zhou, P. B. Wang, B. Zhang, J. C. Zheng, Y. Y. Zhou, C. H. Huang, X. M.

Xi, Suppressing the voltage fading of $Li[Li_{0.2}Ni_{0.13}Co_{0.13}Mn_{0.54}]O_2$ cathode material via Al_2O_3 coating for Li-ion batteries, ***J. Electrochem. Soc.***, 165 (2018) A1648-A1655.

[37] W. Liu, M. Wang, X. L. Gao, W. D. Zhang, J. T. Chen, H. H. Zhou,X. X. Zhang, Improvement of the high-temperature, high-voltage cycling performance of $LiNi_{0.5}Co_{0.2}Mn_{0.3}O_2$ cathode with TiO_2 coating, ***J. Alloys Compd.***, 543 (2012) 181–188.

[38] L. P. Xu, F. Zhou, H. B. Zhou, J. Z. Kong, Q. Z. Wang, G. Z.Yan, $Ti_3C_2(OH)_2$ coated $Li(Ni_{0.6}Co_{0.2}Mn_{0.2})O_2$cathode material with enhanced electrochemical properties for lithium ion battery, ***Electrochim. Acta***, 289 (2018) 120-130.

[39] Z. Li, F. Du, X. F. Bie, D. Zhang, Y. M. Cai, X. R. Cui, C. Z. Wang, G. Chen, Y. J. Wei, Electrochemical kinetics of the $Li[Li_{0.23}Co_{0.3}Mn_{0.47}]O_2$ cathode material studied by GITT and EIS, ***J. Phys. Chem. C***, 114 (2010) 22751-22757.

[40] L. C. Chen, Y. M. Yang, Z. S. Wang, Z. Y. Lin, J. Y. Zhang, Q. L. Su, Y. Chen, W. Chen, Y. B. Lin, Z. G. Huang, Enhanced electrochemical performances and thermal stability of $LiNi_{1/3}Co_{1/3}Mn_{1/3}O_2$ by surface modification with YF_3, ***J. Alloys Compd.***, 711 (2017) 462-472.

[41] S.C. Nagpure, B. Bhushan, S.S. Babu, Surface potential measurement of aged Li-ion batteries using Kelvin probe microscopy, ***J. Power Sources***, 196 (2011) 1508-1512.

[42] Z. Y. Lin, G. Z. Liu, Y. P. Zheng, Y. B. Lin, Z. G. Huang, Three-dimensional hierarchical mesoporous flower-like TiO_2@graphdiyne with superior electrochemical performances for lithium-ion batteries, ***J. Mater. Chem. A***, 6 (2018) 22655-22661.

[43] B. Bhushan, Scanning probe microscopy in nanoscience and nanotechnology, Springer Heidelberg, Dordrecht London New York, 2017, 46.

[44] J. B. Goodenough, K. S. Park, The Li-ion rechargeable battery: A perspective, ***J. Am. Chem. Soc.***, 135 **(2013)** 1167−1176.

[45] Q. Fu, F. Du, X. F. Bian, Y. H. Wang, X. Yan, Y. Q. Zhang, K. Zhu, G. Chen, C. Z. Wang, Y. J. Wei, Electrochemical performance and thermal stability of $Li_{1.18}Co_{0.15}Ni_{0.15}Mn_{0.52}O_2$ surface coated with the ionic conductor Li_3VO_4, ***J. Mater. Chem. A***, 2 (2014) 7555-7562.

[46] S. Hu, Y. Li, Y. Chen, J. Peng, T. Zhou, W. K. Pang, C. Didier, V.K. Peterson, H. Wang, Q. Li, Z. Guo, Insight of a phase compatible surface coating for long-durable Li-rich layered oxide cathode, ***Adv. Energy Mater.***, 9 (2019) 1901795.

[47] N. Yabuuchi, K. Yoshii, S.-T. Myung, I. Nakai, S. Komaba, Detailed studies of a high-capacity electrode material for rechargeable batteries, Li_2MnO_3-$LiCo_{1/3}Ni_{1/3}Mn_{1/3}O_2$, ***J. Am. Chem. Soc.***, 133 (2011) 4404-4419.

[48] L. Ma, Y. Li, Z. Chen, F. Zhang, P. Ding, L. Mao, F. Lian, Improved rate capability of Li-rich cathode materials by building a Li^+-conductive Li_xBPO_4+x/2 nanolayer from residual Li_2CO_3 on the surface, ***ChemElectroChem***., 4 (2017) 1443-1449.

[49] J. L. Shi, D. D. Xiao, M. Ge, X. Yu, Y. Chu, X. Huang, X. D. Zhang, Y. X. Yin, X. Q. Yang, Y. G. Guo, L. Gu, L. J. Wan, High-capacity cathode material with high voltage for Li-ion batteries, ***Adv. Mater.***, 30 (2018) 1705575.

[50] M. Hekmatfar, A. Kazzazi, G.G. Eshetu, I. Hasa, S. Passerini, Understanding the electrode/electrolyte interface layer on the Li-rich nickel manganese cobalt layered oxide cathode by XPS, ***ACS Appl. Mater. Interfaces***, 11 (2019)

43166-43179.

[51] M. Vivekanantha, C. Senthil, T. Kesavan, T. Partheeban, M. Navaneethan, B. Senthilkumar, P. Barpanda, M. Sasidharan, Reactive template synthesis of $Li_{1.2}Mn_{0.54}Ni_{0.13}Co_{0.13}O_2$ nanorod cathode for Li-ion batteries: Influence of temperature over structural and electrochemical properties, ***Electrochim. Acta,*** 317 (2019) 398-407.

[52] L. Ku, Y. X. Cai, Y. T. Ma, H. F. Zheng, P. F. Liu, Z. S. Qiao, Q. S. Xie, L. S. Wang, D. L. Peng, Enhanced electrochemical performances of layered-spinel heterostructured lithium-rich $Li_{1.2}Ni_{0.13}Co_{0.13}Mn_{0.54}O_2$ cathode materials, ***Chem. Engin. J.***, 370 (2019) 499–507.

[53] C. Liu, M. M. Wu, Y. H. Zong, L. Zhang, Y. Yang, G. Yang, Synthesis and structural properties of xLi_2MnO_3,(1-x)$LiNi_{0.5}Mn_{0.5}O_2$ single crystals towards enhancing reversibility for lithium-ion battery/pouch cells, ***J. Alloys Compd.***, 770 (2019) 490-499.

[54] H. Chen, L. Wu, F. Bo, J. Jian, L. Wu, H. Zhang, L. Zheng, Y. Kong, Y. Zhang, J. Xu, Coexistence of self-reduction from Mn^{4+} to Mn^{2+} and elastic-mechanoluminescence in diphase $KZn(PO_3)_3$:Mn^{2+}, ***J. Mater. Chem. C***, 7 (2019) 7096-7103.

[55] J. Zheng, M. Gu, J. Xiao, P. Zuo, C. Wang, J.-G. Zhang, Corrosion/fragmentation of layered composite cathode and related capacity/voltage fading during cycling process, ***Nano Lett.***, 13 (2013) 3824-3830.

[56] M. Gu, Y. He, J. M. Zheng, C. M. Wang, Nanoscale silicon as anode for Li-ion batteries: The fundamentals, promises, and challenges, ***Nano Energy***, 17 (2015) 366-383.

[57] B. Li, R. Qi, J. Zai, F. Du, C. Xue, Y. Jin, C. Jin, Z. Ma, X. Qian, Silica wastes to

high-performance lithium storage materials: a rational designed Al_2O_3 coating assisted magnesiothermic process, ***Small.***, 12 (2016) 5281–5287.

[58] K. Tasaki, A. Goldberg, J.-J. Lian, M. Walker, A. Timmons, S.J. Harris, Solubility of lithium salts formed on the lithium-ion battery negative electrode surface in organic solvents, ***J. Electrochem. Soc.***, 156 (2009) A1019-A1027.

[59] H. Yildirim, A. Kinaci, M.K.Y. Chan, J.P. Greeley, First-principles analysis of defect thermodynamics and ion transport in inorganic SEI compounds: LiF and NaF, ***ACS Appl. Mater. Interfaces***. 7 (2015) 18985–18996.

Figure Captions

Fig. 1 Schematic illustration of the synthesis of TiO_2-modified LLCNMO samples.

Fig. 2 SEM images of the (a) LLNCMO and (b) LLNCMO@TiO_2 powders; (c) XRD patterns of LLNCMO and LLNCMO@TiO_2 powders; (d-f) HR-TEM images and (g-l) EDS mappings of LLNCMO@TiO_2 powders.

Fig. 3 (a) The initial charge and discharge curves of LLNCMO and LLNCMO@TiO_2 electrodes; (b) Rate capability of LLNCMO and LLNCMO@TiO_2 electrodes from 0.2 C to 5 C; (c,d) Discharge curves of the LLNCMO and LLNCMO@TiO_2 electrodes at 0.2, 0.5, 1, 2, 3 and 5C respectively.

Fig. 4 Cyclic performances of LLNCMO and LLNCMO@TiO_2 electrodes at 1C at (a) 25 ^oC and (b) 55 ^oC; CV curves of (a) LLNCMO and (b)LLNCMO@TiO_2 electrodes at a scanning rate of 0.1 mVs^{-1}.

Fig. 5 (a) EIS of LLNCMO and LLNCMO@TiO_2 at full charged state after 100 cycles, Inset: the equivalent circuit for fitting; GITT potential profiles of (b) LLNCMO and (c) LLNCMO@TiO_2 electrodes for lithiation process during the 100th charge process; (d) Li-ion diffusion coefficients calculated from the GITT potential profiles.

Fig. 6 EIS for (a) LLNCMO and (b) LLNCMO@TiO_2 at the full-charged state at different operation temperatures; (c) Profile of log (Rct) vs. temperature for LLNCMO and LLNCMO@TiO_2 electrodes; (d) image figure of improvement of activation energy by TiO_2-coating.

Fig. 7 (a) The work electrode consisting of LLNCMO and LLNCMO@TiO_2 for testing surface potential; Work function of (b) LLNCMO and (c) LLNCMO@TiO_2 at different charged state; (d) Comparison of Work

function for LLNCMO and LLNCMO@TiO_2 particles.

Fig. 8 **(a)** Potential energy diagram for LLNCMO and LLNCMO@TiO_2 with different work functions, which are initially not connected and share thus a common vacuum level; (**b)** If LLNCMO and LLNCMO@TiO_2 are connected, the Fermi levels of the two composites align. A build-up of surface charge leads to a potential gradient compensating the difference between the work functions of the two composites; (c) the relative energies of the electrolyte window and HOMO of cathode material; (d) DSC profiles of LLNCMO and LLNCMO@TiO_2 at full charged state.

Fig. 9 (a,b) O 1s, (c,d) C 1s and (e,f) Mn 2p XPS spectra of LLNCMO and LLNCMO@TiO_2 extracted from coin cells after 100 charge/discharge cycles, respectively.

Fig. 10 (a, b) F 1s, (c, d) P 2p XPS spectra and (e, f) of the relative content of elements in LLNCMO and LLNCMO@TiO_2 electrodes after 100 charge/discharge cycles respectively.

Declaration of Interest Statement

☒ The authors declare that they have no known competing financial interests or personal relationships that could have appeared to influence the work reported in this paper.

☐The authors declare the following financial interests/personal relationships which may be considered as potential competing interests:

Xinxin Ran, Jianming Tao, Ziyan Chen, Jerui Yan, Yanmin Yang, Jiaxin Li, Yinbin Lin, Zhigao Huang

Credit Author Statement

Author contributions

Xinxin Ran: Investigation, Preparation and characterization of cathode materials, Battery testing, Writing - Original Draft.

Jianming Tao: Investigation on the potential mechanism on improved in terms of XPS, KP-AFM.

Ziyan Chen: Preparation of cathode materials, Battering assembling.

Zerui Yan: Preparation of cathode materials, Battery testing.

Yanmin Yang: Build theoretical model for explanation mechanism.

Jiaxin Li: Supervision, Data Curation.

Yingbin Lin: Resources, Supervision, Data Curation, Writing: Review & Editing.

Zhigao Huang: Writing: Review & Editing.

Figure 1

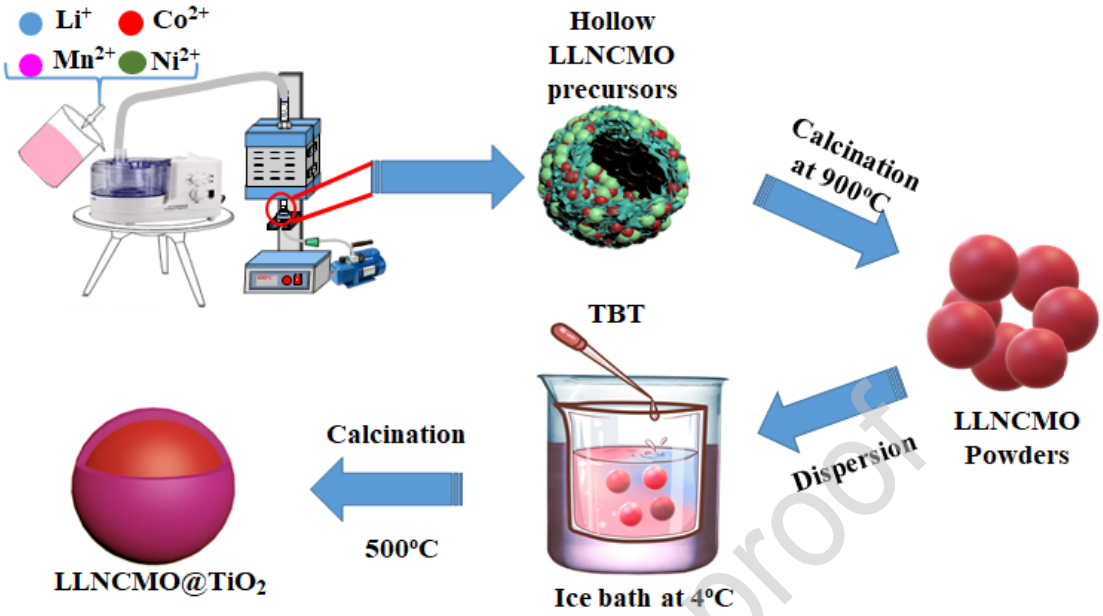

Figure 2

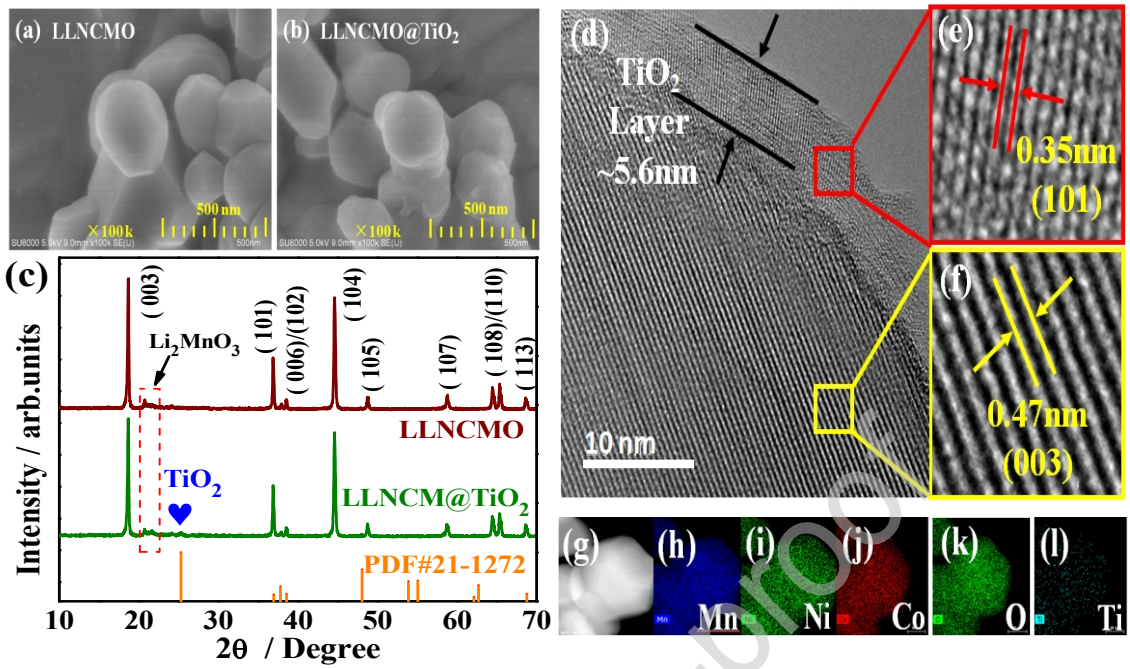

Figure 3

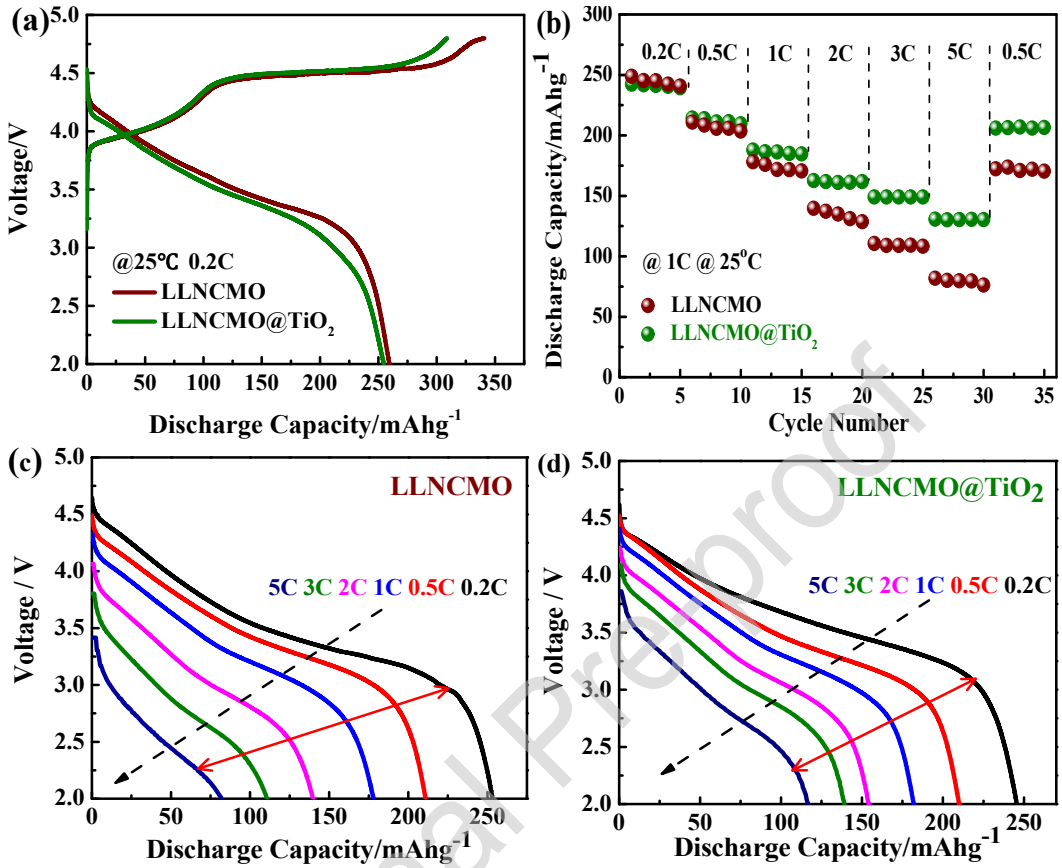

Figure 4

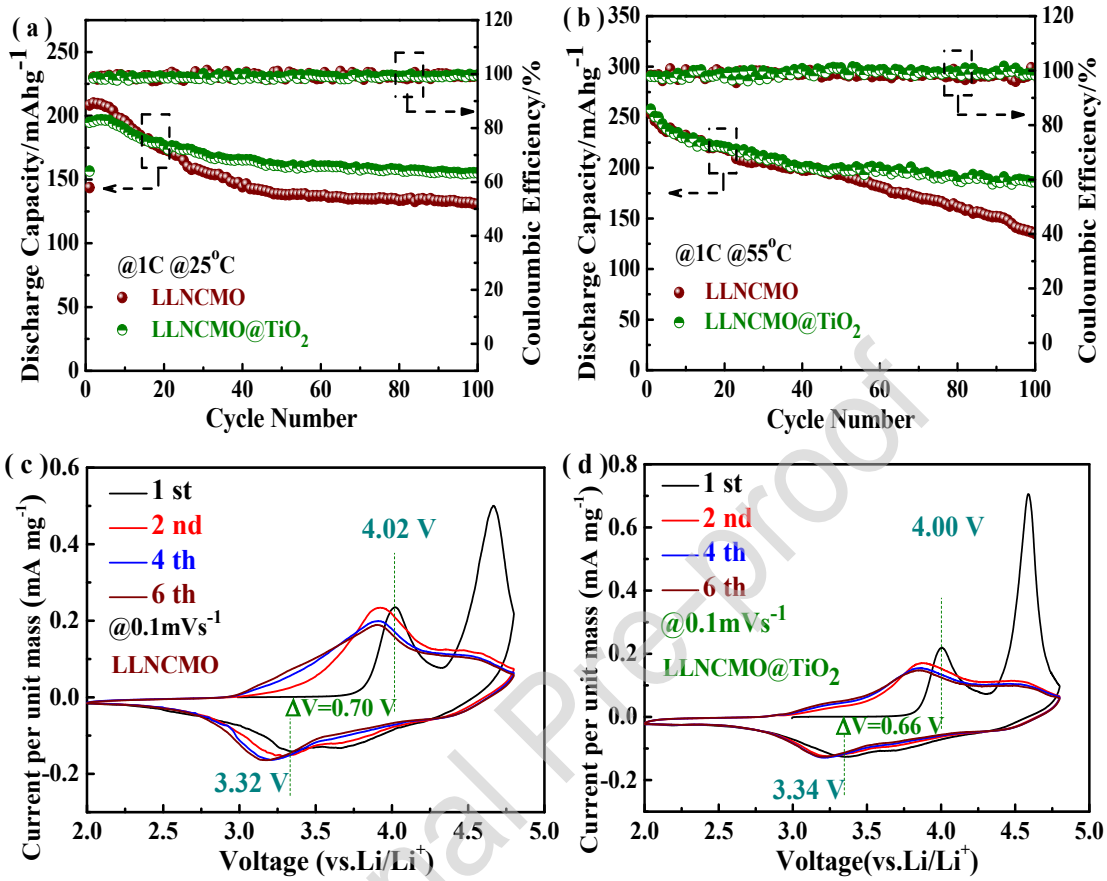

Figure 5

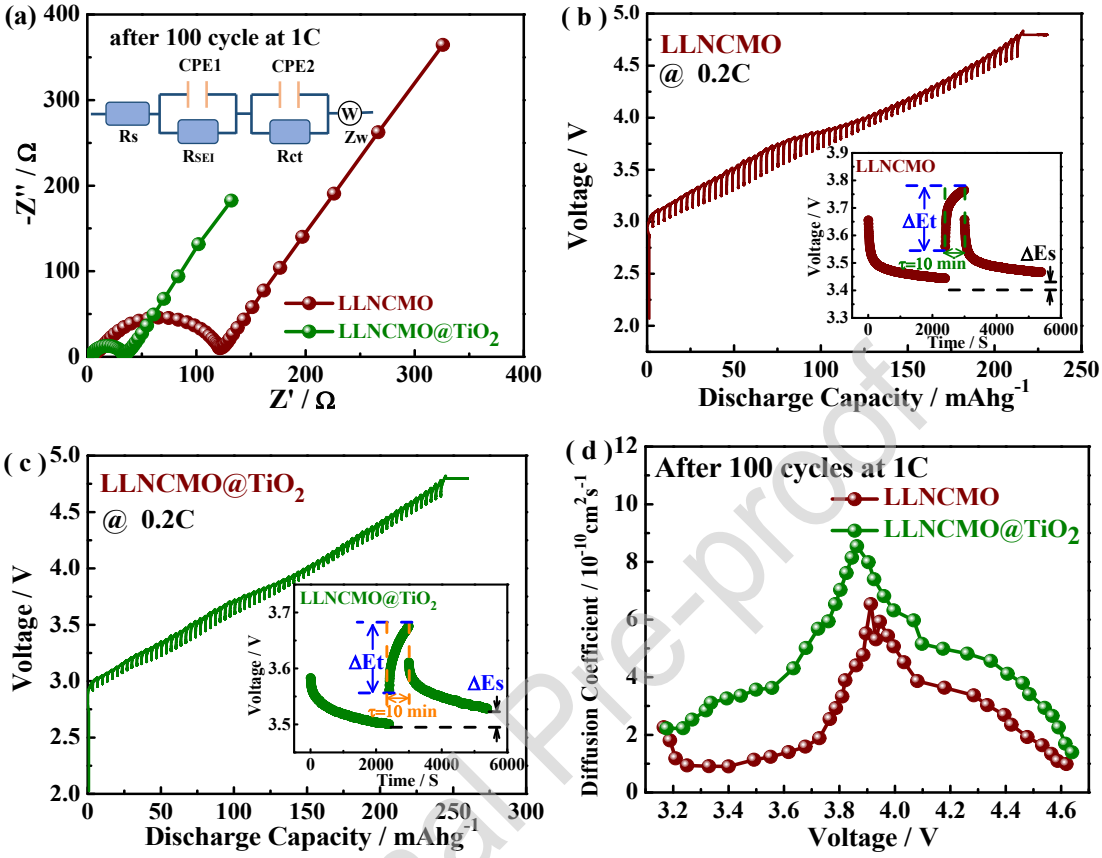

Figure 6

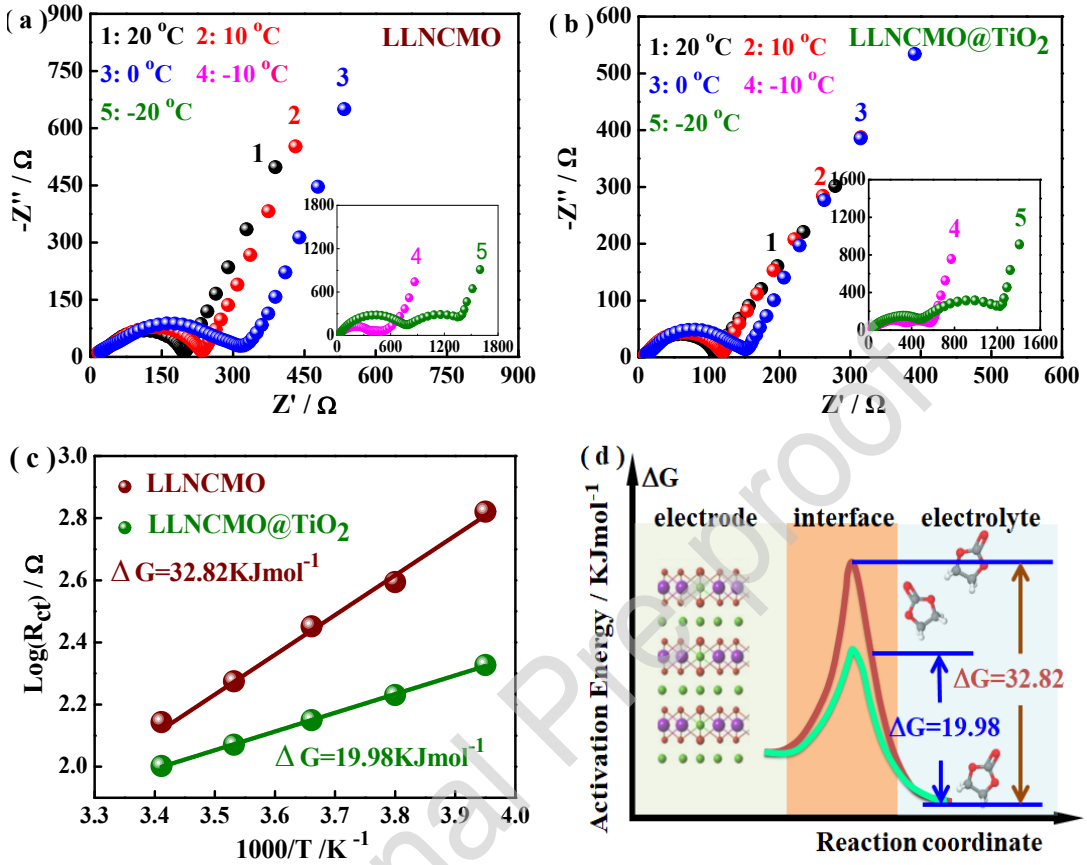

Figure 7

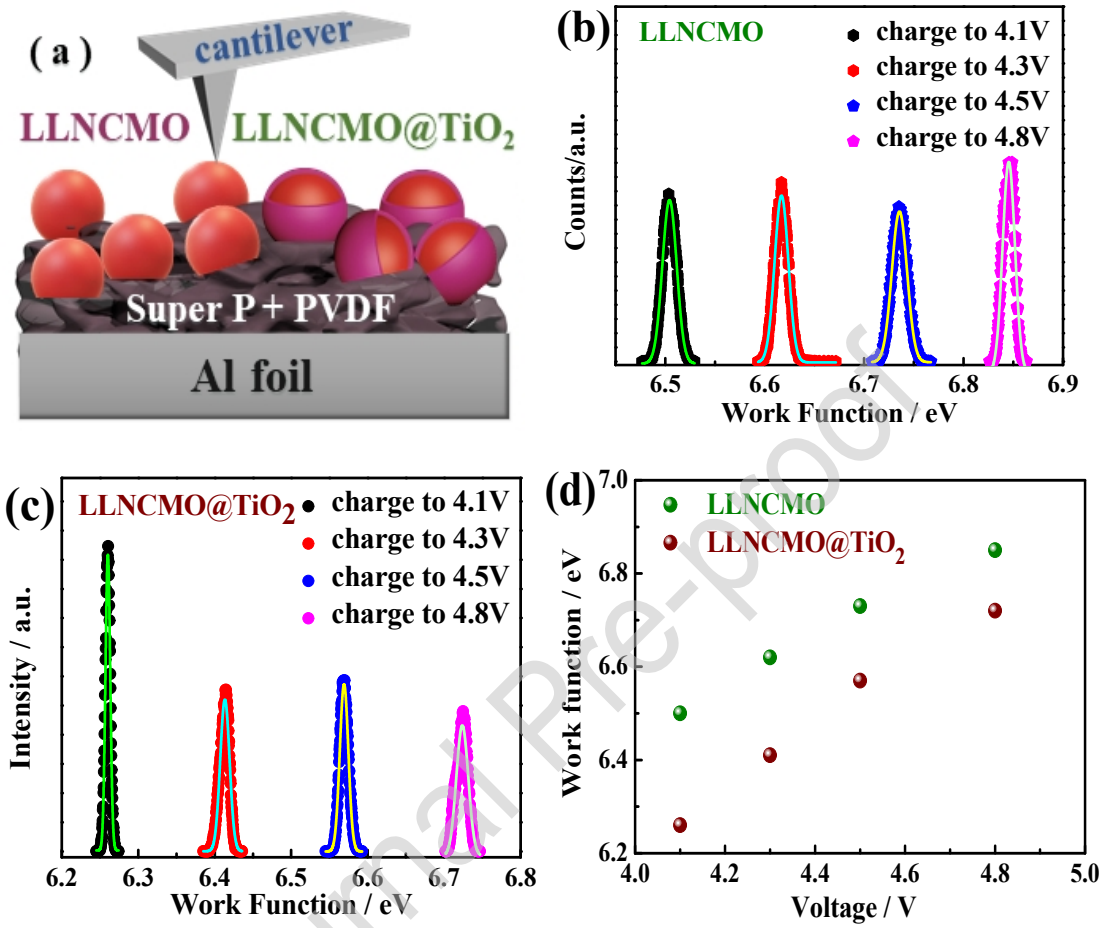

Figure 8

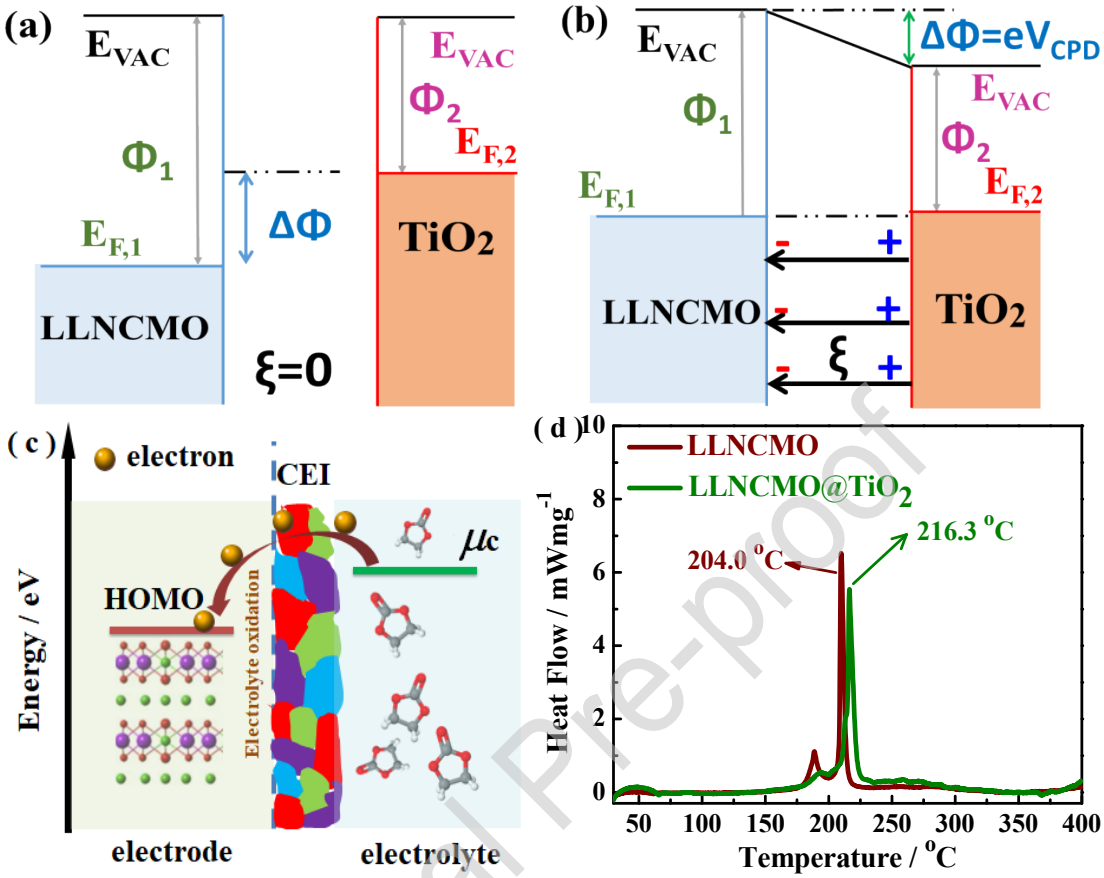

Figure 9

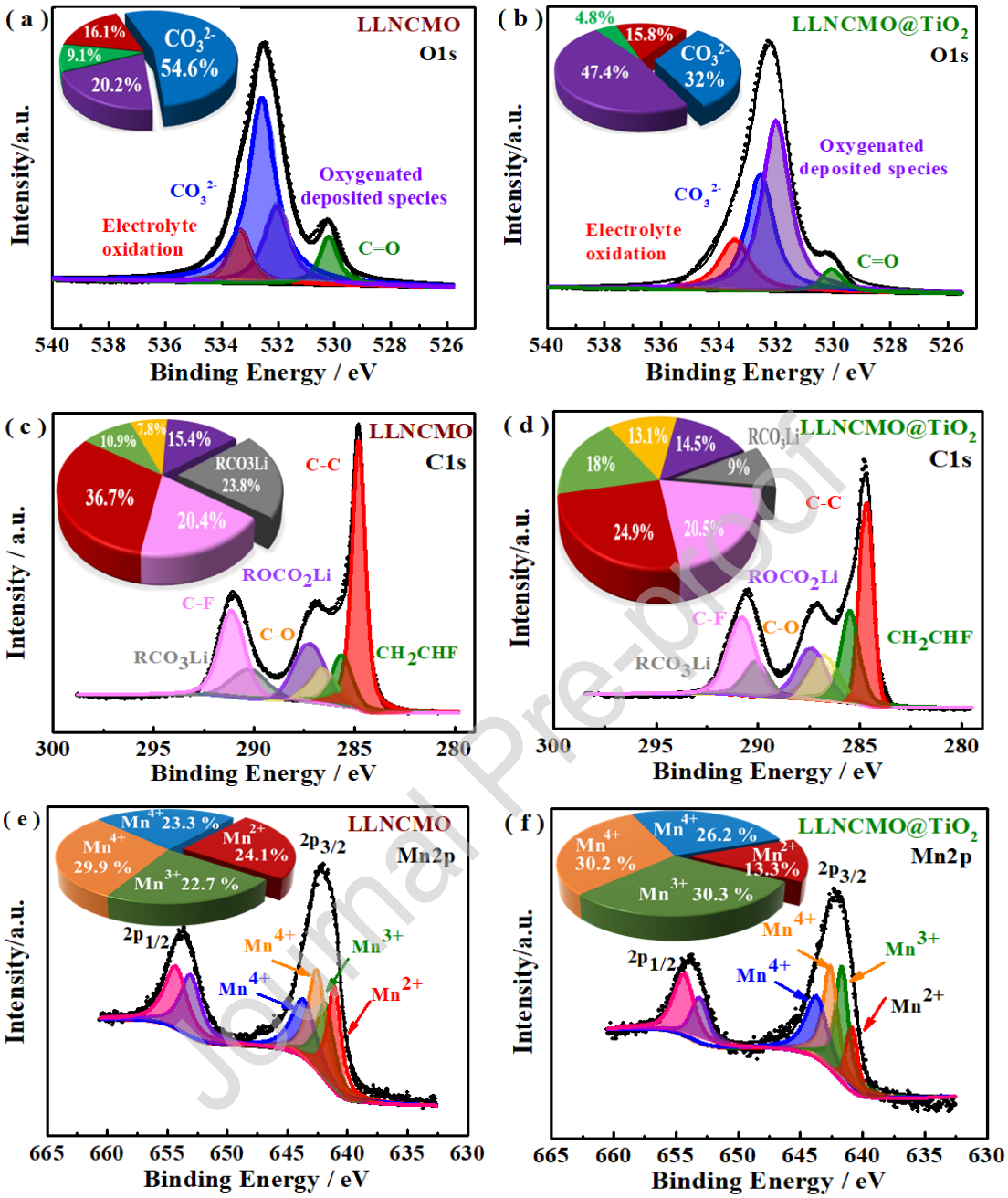

Figure 10

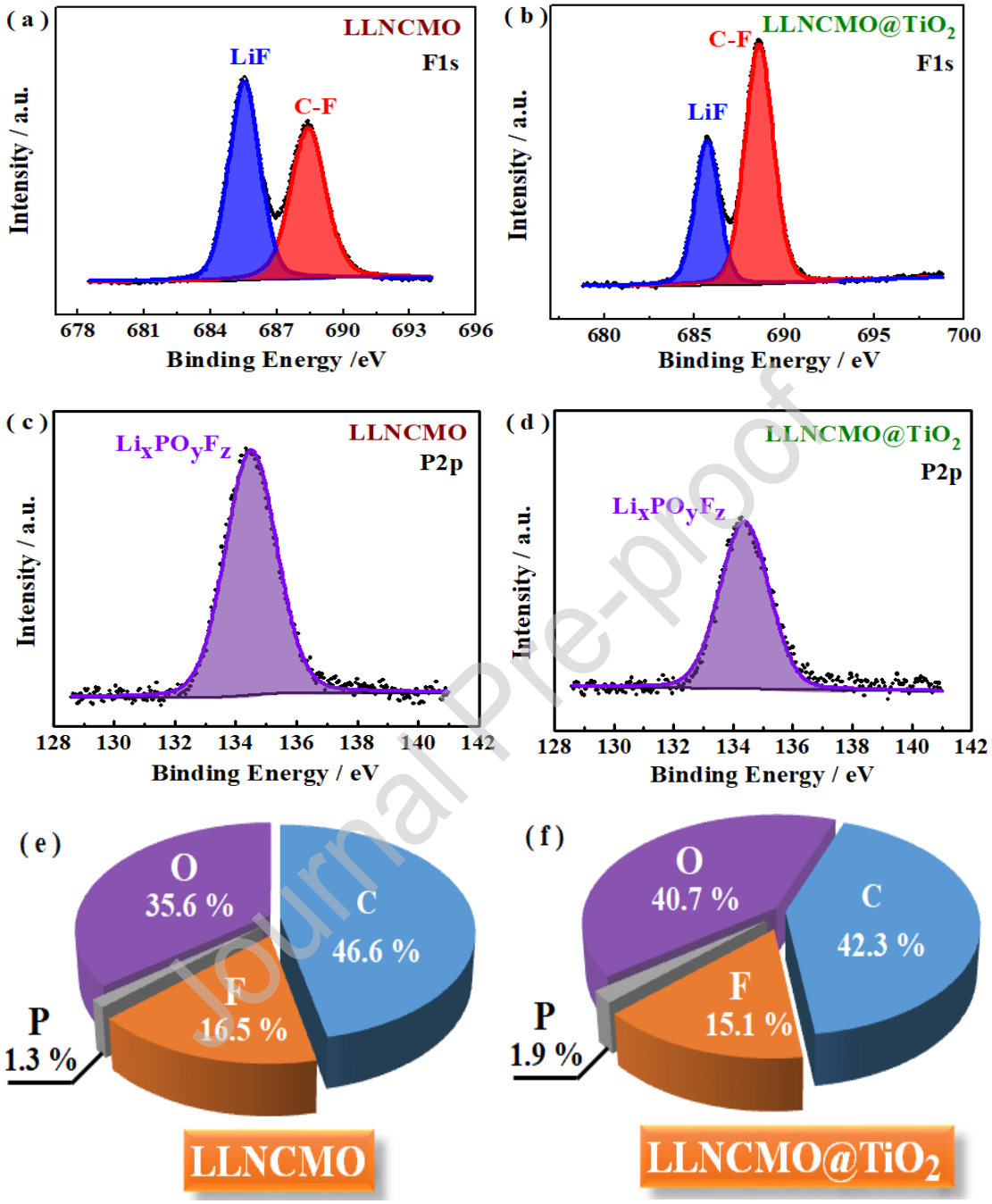

Research highlights

- Heterostructural $Li_{1.2}Ni_{0.13}Co_{0.13}Mn_{0.54}O_2$@$TiO_2$ composites are prepared via low-temperature hydrolysis.
- The electrochemical performances are improved by TiO_2-coating in terms of rate capability, cycling stability and thermal stability.
- The different in work function of composite facilitates charges across the heterojunction interface and relieves electrolyte decomposition.